

**Resonant Raman spectroscopy of (Mn,Co)-codoped ZnO films**C. L. Du,<sup>1,a)</sup> Z. B. Gu,<sup>2</sup> Y. M. You,<sup>1</sup> J. Kasim,<sup>1</sup> T. Yu,<sup>1</sup> Z. X. Shen,<sup>1</sup> Z. H. Ni,<sup>1</sup> Y. Ma,<sup>1</sup> G. X. Cheng,<sup>3</sup> and Y. F. Chen<sup>3</sup><sup>1</sup>*Division of Physics and Applied Physics, School of Physical and Mathematical Sciences, Nanyang Technological University, Singapore 637616, Singapore*<sup>2</sup>*National Laboratory of Solid State Microstructures, Department of Materials Science and Engineering, Nanjing University, Nanjing 210093, China*<sup>3</sup>*National Laboratory of Solid State Microstructures, Nanjing University, Nanjing 210093, China*

(Received 22 August 2007; accepted 26 November 2007; published online 31 January 2008)

Resonant Raman spectroscopy studies of (Mn, Co)-codoped ZnO films were carried out using the 325 nm laser as the excitation source. The mixed mode character of the longitudinal optical (LO) phonon reveals that the resonant Raman spectra of the films can be used to test the *c*-axis orientation degree of their crystallite grains. The ratio of integrated Raman intensities between the 2LO to LO changes as a function of annealing temperatures, which reaches maximum at about 800 °C and demonstrates the variation of electron-LO phonon coupling in the films. These can provide helpful information for the fabrication of ZnO based functional films and for the development of their future applications. © 2008 American Institute of Physics. [DOI: 10.1063/1.2837110]

**I. INTRODUCTION**

The potential applications of magnetic-ion-doped ZnO films in spintronics have attracted much attention recently since they are highly desirable candidates for diluted magnetic semiconductors (DMS) to realize room-temperature ferromagnetism.<sup>1,2</sup> Understanding phonon and structural properties of such films is important from the fundamental physics point of view, which may in turn help to improve the material quality. Raman scattering has been widely used to study ZnO based compounds.<sup>3–13</sup> Especially owing to the associated macroscopic field, the polar longitudinal optical (LO) phonon mode can couple with electrons, which affects semiconductor optoelectronic properties consequently. Furthermore, LO phonon modes usually are regarded as mixed modes, i.e., superposition of  $A_1$  LO and  $E_1$  LO phonon modes, due to that Raman scattering from sample (films herein) axes does not overlap exactly with crystal-symmetry axes (*a* or *c* axis of the wurtzite structure).<sup>13</sup> It is noted that resonant Raman spectra (RRS) study on LO phonon modes could provide some information about the degree for such overlapping. RRS of ZnO based samples can also provide information about electron-phonon interactions.<sup>14–17</sup> (Mn, Co)-codoped ZnO films with room-temperature ferromagnetism have been grown and the origins of their different phonon modes were also discussed previously.<sup>18,19</sup> In the present work, RRS of the codoped ZnO films were studied to reveal their phonon and structural properties. The results demonstrate that the RRS can be used to study the variation of both the electron-phonon coupling and the deformation energy as functions of postannealing temperature and also to test the high quality of the *c*-axis textured films.

**II. EXPERIMENT**

The (Mn, Co)-codoped ZnO DMS films were grown on *c*-sapphire (0001) and silicon (001) by a radio frequency

magnetic sputtering system with  $Zn_{0.95}Mn_{0.05}O$  and  $Zn_{0.80}Co_{0.20}O$  targets. The deposition temperature was 550 °C in argon ambient. The experimental details have been given elsewhere.<sup>18,19</sup> Raman and resonant Raman spectra of the films were recorded in backscattering geometry using a JY LabRam HR800 spectrometer. An argon ion laser (488 nm) and a He–Cd laser (325 nm) were adopted as the excitation sources. The crystal structure and the chemical composition of the cosputtered films have been investigated previously by x-ray diffraction (XRD) and x-ray photoelectron spectroscopy.<sup>18</sup> The results reveal that the films are *c*-axis textured and the magnetic ions substitute the  $Zn^{2+}$  sites in the crystal lattice. Their chemical composition is measured to be  $(Mn_{0.03}Co_{0.07})Zn_{0.90}O$  (abbreviated as ZnMn-CoO). The absorption spectra of the films were measured at room temperature on an ultraviolet-visible (UV-VIS) spectrometer.

**III. RESULTS AND DISCUSSION**

Using the biaxial strain model,<sup>20</sup> the strain in the films along *c*-axis  $\varepsilon = (c_{\text{film}} - c_{\text{bulk}}) / c_{\text{bulk}}$  is calculated to be  $9.75 \times 10^{-2}\%$  and  $5.57 \times 10^{-2}\%$  for films deposited on sapphire (sample A) and on silicon (sample B), respectively, where the lattice constant of the film  $c_{\text{film}}$  is derived from their corresponding XRD pattern<sup>18</sup> while  $c_{\text{bulk}}$  is the lattice constant *c* of ZnO single crystal. This strain is believed to be small enough and its effect on the Raman and resonant Raman spectra are neglected accordingly.

The origins of the different phonon modes of the Raman spectra of the ZnMnCoO films have been discussed elsewhere.<sup>19</sup> Here we just briefly give the results for completion. Figure 1 gives the Raman spectra of samples A and B along with the spectra of the undoped ZnO films and ZnO single crystal for comparison. The Mn, Co codoping effect on the spectra was revealed by the presence of additional phonon modes at 275 and 642  $cm^{-1}$  and another intensive phonon mode at around 524  $cm^{-1}$ .<sup>19</sup> Compared with the Ra-

<sup>a)</sup>Electronic mail: cldu@ntu.edu.sg.

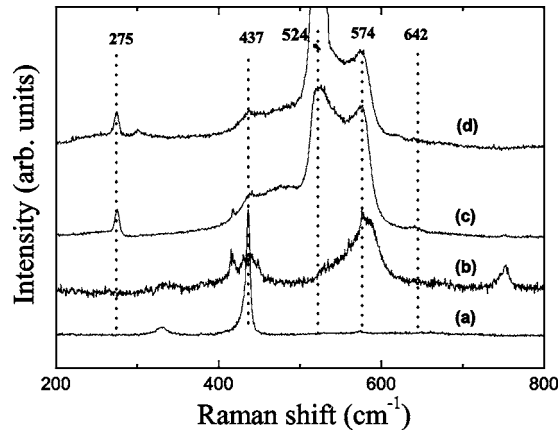


FIG. 1. Raman spectra of ZnO single crystal from the *c* face (a), ZnO/sapphire film (b), ZnMnCoO/sapphire film (sample A) (c), and ZnMnCoO/silicon film (sample B) (d). The wavelength of the excitation laser is 488 nm.

man spectra of ZnO single crystal from the *c* face, only  $E_2$  high ( $437\text{ cm}^{-1}$ ) and  $A_1$  LO ( $574\text{ cm}^{-1}$ ) phonon mode are detected for samples A and B. This indicates that the films have the same hexagonal structure as the single crystal and also confirms their *c*-axis orientated texture. Furthermore, it is noted that the frequencies of these two phonon modes of both samples A and B coincide with those of ZnO single crystal. The absence of their Raman peak shifts indicates neglectful strain between the film and substrate, which is consistent with the analysis from XRD results.

Resonant Raman scattering occurs when the films are excited by 325 nm laser line.<sup>19</sup> The RRS of the samples A and B are shown in Fig. 2 together with that of ZnO single crystal from the *c* face. As can be seen from the inset, the direct band gap of sample A is about 2.8 eV, measured by the UV-VIS absorption spectrometer. For the RRS of the hexagonal structures, total Raman cross section of the *n*-LO phonon process can be expressed as<sup>21</sup>

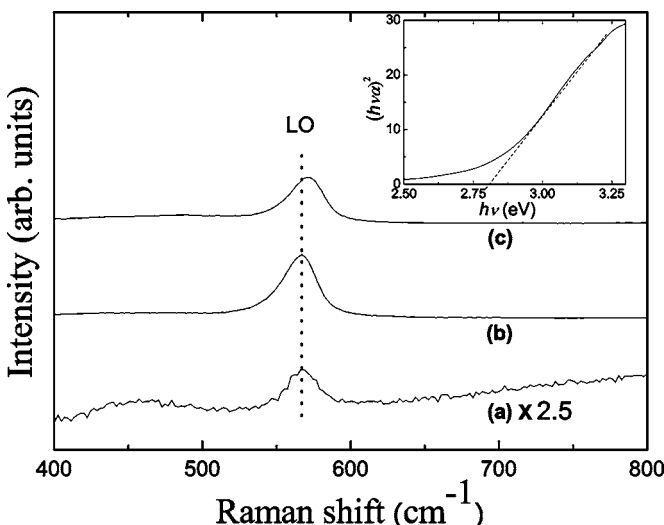


FIG. 2. Resonant Raman spectra of the ZnO single crystal from the *c* face (a), sample A (b), and sample B (c). The inset shows the UV-VIS absorption spectra of sample A, from which the absorption edge of the film is estimated to be about 2.8 eV.

$$\sigma_n = \int \sigma_n^R(\omega) f(R) dR, \quad (1)$$

$$\sigma_n^R(\omega) = \mu^4 \left| \sum_{m=0}^{\infty} \frac{\langle n|m\rangle \langle m|0\rangle}{E_e + n\hbar\omega_{LO} - \hbar\omega + i\hbar\Gamma} \right|^2 \times \exp\left(-\frac{i\hbar\omega_{LO}}{k_B T}\right), \quad (2)$$

where  $n$ ,  $\mu$ ,  $E_e$ ,  $\hbar\omega$ , and  $\hbar\omega_{LO}$  are the order of LO phonon, the electronic dipole transition moment, the excited-state energy, the incident photon energy, and the LO phonon energy, respectively, while  $m$ ,  $\Gamma$ ,  $k_B$ , and  $T$  are the intermediate vibration level in the excited state, the homogeneous linewidth, Boltzmann constant, and temperature, respectively. The RRS intensity can be enhanced when the energies of the incident or the scattered photons match with the real electronic state  $E_e$  in the material and thus cause the denominator in Eq. (2) to reach the minimum. In the present case, the single photon energy of the incident laser is about 1 eV higher than the band gap of the sample. It means that there is a case of incoming resonance, where the laser line is in resonance with an interband electronic transition.<sup>14–17</sup>

It is interesting to note that the frequency of the 1LO phonon mode of the ZnMnCoO films in Fig. 2 almost coincides with that of ZnO single crystal as indicated by the dotted lines, in good agreement with Ref. 13. The Raman frequency of the polar LO phonon mode ( $\omega_{LO}$ ) in the RRS for hexagonal structure can usually be written as<sup>22</sup>

$$\omega_{LO}^2 = \omega_{A_1 LO}^2 \cos^2(\theta) + \omega_{E_1 LO}^2 \sin^2(\theta), \quad (3)$$

i.e., the frequency of the LO mode is determined by the angle ( $\theta$ ) between the phonon wave vector  $\mathbf{q}$  and the crystal symmetry axis *c*, where  $\omega_{A_1 LO}$  and  $\omega_{E_1 LO}$  can be obtained from the RRS of ZnO single crystal. Based on Eq. (3), the coincidence of the LO phonon mode frequency in the RRS of sample A with that of the  $A_1$  LO mode of the ZnO single crystal indicating that  $\theta$  approximates to zero. Consequently, the LO mode can be assumed as  $A_1$  LO and confirms the high *c*-axis orientation for the crystallite grains in the film as well. Sample B also exhibits *c*-axis texture as revealed by their XRD (not shown). However, in its RRS,  $\omega_{LO}$  is  $4\text{ cm}^{-1}$  higher than  $\omega_{A_1 LO}$ . By using Eq. (3),  $\theta$  is calculated to be about  $28^\circ$  for sample B, implying that the crystalline grains in the film are tilted by an average angle of  $28^\circ$  with respect to the *c* axis. The earlier results show that the degree of *c*-axis orientation for sample A is apparently larger than that for sample B, within which the crystalline grains are tilted to the *c* axis, leading to the mixed-mode character of the RRS LO phonon mode. The difference between the XRD results and the RRS is due to the fact that the XRD  $\theta$ - $2\theta$  patterns primarily depends on the coherent separation of Zn planes while in contrast Raman scattering is very sensitive to the loss of transitional symmetry in materials, such as tilting crystalline grains. These indicate that the RRS can be used to test the quality of the *c*-axis textured ZnO based films.

The RRS of the postannealed sample A are also presented in Fig. 3 along with that of the as-deposited film. As

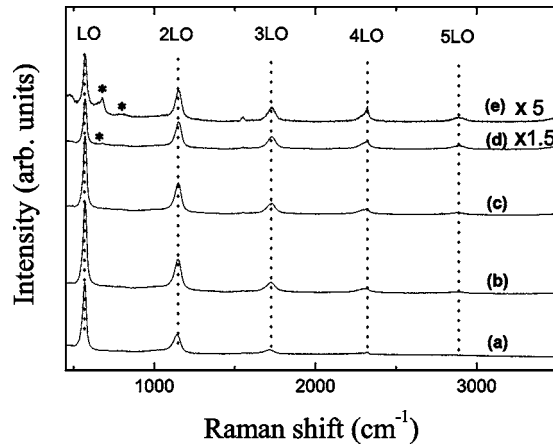


FIG. 3. Resonant Raman spectra of the as-deposited sample A (a), and its postannealed samples heated at 400 (b), 600 (c), 800 (d), and 900 (e) for 1 h in air, respectively.

shown, up to five-order LO phonon modes are observed, revealing the large polaron coupling coefficient  $\alpha$  for the films since  $\alpha$  varies monotonically with the number of multiple phonon modes  $n(\text{LO})$  observed in semiconductors.<sup>23</sup> On the other hand, the maximum frequency shift  $n(\text{LO})\omega_{\text{LO}}$  can be compared with the deformation energy in the material.<sup>23</sup> The high frequency for the highest order LO in the RRS, 5-LO in this work, indicates that ZnMnCoO/sapphire film has large deformation energy. Furthermore, the order ( $n=5$ ) and corresponding frequency of LO are almost independent of the annealing temperature as can be seen from the dotted lines in Fig. 3, implying that the deformation energy of the ZnMnCoO/sapphire film does not change with annealing. Figure 3 also shows that the integrated Raman intensity of first LO phonon ( $I_{\text{LO}}$ ) is larger than that of second LO phonon ( $I_{2\text{LO}}$ ), which is contrary to ZnO single crystal case. This may be due to that the impurity or defect scatters, which give contributions to the RRS as well.<sup>24</sup> It is also noted that both  $I_{\text{LO}}$  and  $I_{2\text{LO}}$  increase when the annealing temperature increasing up to 600 °C and then decrease with further increasing temperatures. It is known that the Raman intensity ( $R_i$ ) in RRS correlates closely with laser lines, grain size, temperatures, and band gaps of samples. With postannealing the sample at high temperature, the average grain size increases, defects such as oxygen vacancies and Zn interstitials decrease, and thus the film crystal quality becomes better. Meanwhile, the sample structure changes accordingly. Its band gap increases with the annealing temperature increasing as revealed by their corresponding photoluminescence spectra (not shown), which is similar to literature.<sup>14</sup> Consequently, increasing the postannealing temperature results in the redistribution of the intensity of lines in the RRS favoring more phonons participation scattering. This can explain the enhancement of  $R_i$  of LO and 2LO up to 600 °C. However, with temperature increasing higher to 800 and 900 °C, their intensity decreases. It may be owing to the segregation of  $\text{Mn}^{2+}$  and  $\text{Co}^{2+}$  from the crystal, which can lead to impurity phases as revealed by some new RRS peaks labeled by stars (\*) in Fig. 3. The  $I_{2\text{LO}}/I_{\text{LO}}$  ratio as a function of the annealing temperature is plotted in Fig. 4, which reflects the coupling strength between the electron and LO phonon.<sup>23</sup> It

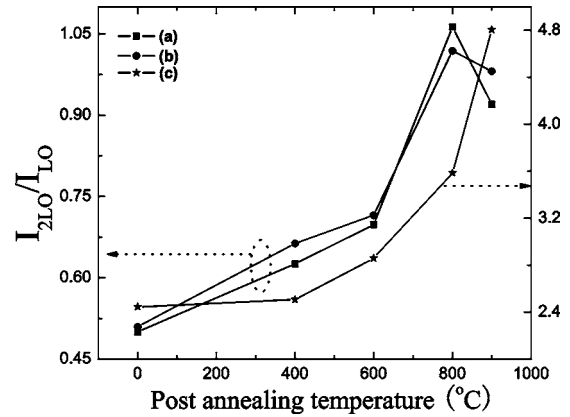


FIG. 4. The ratio of  $I_{2\text{LO}}/I_{\text{LO}}$  as a function of the postannealing temperatures for sample A (a), sample B (b), and undoped ZnO film (c), respectively.

changes with the annealing temperature and reaches maximum at about 800 °C. Generally, electron-LO phonon coupling is determined by the deformation potential and the Fröhlich interaction. It is believed that the variation of Fröhlich interaction induced by the annealing process contributes mainly to the changes of  $I_{2\text{LO}}/I_{\text{LO}}$  ratio considering the unchangeable deformation potential. Additionally, similar  $I_{2\text{LO}}/I_{\text{LO}}$  ratio change is observed for ZnMnCoO/Si film, showing that such change is independent of substrates. For comparison, the  $I_{2\text{LO}}/I_{\text{LO}}$  ratio of undoped ZnO/sapphire films was also plotted in Fig. 4, which increases with the postannealing temperature increasing. The decrease of the ratio at 900 °C of the ZnMnCoO films relative to that at 800 °C may be owing to the  $\text{Mn}^{2+}$  and  $\text{Co}^{2+}$  ions segregation at high temperature worsening the crystal quality. It is also found that the ratio value at different annealing temperatures of ZnO films is always larger than that of ZnMnCoO films, revealing larger electron-LO phonon coupling of ZnO films. As known, the second-order structures are very sensitive to atomic scale disorder, and thus the  $I_{2\text{LO}}/I_{\text{LO}}$  ratio will be decreased by the compositional disorder resulted from the  $\text{Mn}^{2+}$  and  $\text{Co}^{2+}$  ions codoping. Consequently, the electron-LO phonon coupling of the ZnMnCoO films will be weakened.

#### IV. CONCLUSIONS

In summary, both the Raman spectra and resonant Raman spectra results confirm the high quality of the  $c$ -axis oriented ZnMnCoO film deposited on  $c$ -sapphire (0001). The comparison of the RRS between the films deposited on sapphire and silicon substrates indicates that the former exhibits better  $c$ -axis orientation. Compared with the RRS of ZnO single crystal, the smaller  $I_{2\text{LO}}/I_{\text{LO}}$  ratio for ZnMnCoO films reflects the Mn, Co codoping induced composition disorder effect as well as other defect scatters effect on their RRS. With the increase of the postannealing temperature, the  $I_{2\text{LO}}/I_{\text{LO}}$  ratio in RRS reaches maximum at about 800 °C while the order and the frequency of LO phonon unchanged. This is an indicator of the existence of the strongest electron-LO phonon coupling in the samples annealed at about 800 °C, which originates from the variation of Fröhlich interaction within the material. However, the defor-

mation potential of the films is independent of the annealing temperature. These results may provide guideline for fabrication of such films and also be helpful for understanding their correlated properties.

## ACKNOWLEDGMENTS

This work was jointly supported by the State Key Program for Basic Research of China and the National Natural Science Foundation of China (Grant Nos. 50428202 and 10674057), and the Program for Changjiang Scholars and Innovative Research Team in University (PCSIRT).

- <sup>1</sup>T. Dietl, H. Ohno, F. Matsukura, J. Cibert, and D. Ferrand, *Science* **287**, 1019 (2000).
- <sup>2</sup>S. J. Pearton, C. R. Abernathy, D. P. Norton, A. F. Hebard, Y. D. Park, L. A. Boatner, and J. D. Budai, *Mater. Sci. Eng., R.* **40**, 137 (2003).
- <sup>3</sup>J. M. Calleja and M. Cardona, *Phys. Rev. B* **16**, 3753 (1977).
- <sup>4</sup>R. H. Callender, S. S. Sussman, M. Selders, and R. K. Chang, *Phys. Rev. B* **7**, 3788 (1973).
- <sup>5</sup>C. Bundesmann, N. Ashkenov, M. Schubert, D. Spemann, T. Butz, E. M. Kaidashev, M. Lorenz, and M. Grundmann, *Appl. Phys. Lett.* **83**, 1974 (2003).
- <sup>6</sup>N. Hasuike, H. Fukumura, H. Harima, K. Kisoda, H. Matsui, H. Saeki, and H. Tabata, *J. Phys.: Condens. Matter* **16**, S5807 (2004).
- <sup>7</sup>L. W. Yang, X. L. Wu, G. S. Huang, T. Qiu, and Y. M. Yang, *J. Appl. Phys.* **97**, 014308 (2005).
- <sup>8</sup>M. Tzolov, N. Tzenov, D. Dimova-Malinovska, M. Kalitzova, C. Pizzuto,

- G. Vitali, G. Zollo, and I. Ivanov, *Thin Solid Films* **379**, 28 (2000).
- <sup>9</sup>S. K. Sharma and G. J. Exarhos, *Solid State Phenom.* **55**, 32 (1997).
- <sup>10</sup>J. M. Liu, C. K. Ong, and L. C. Lim, *Ferroelectrics* **231**, 223 (1999).
- <sup>11</sup>N. H. Nickel, F. Friedrich, J. F. Rommeluère, and P. Galtier, *J. Appl. Phys.* **87**, 211905 (2005).
- <sup>12</sup>A. Kaschner, U. Haboeck, M. Strassburg, M. Strassburg, G. Kaczmrczky, A. Hoffmann, C. Thomsen, A. Zeuner, H. R. Alves, D. M. Hofmann, and B. K. Meyer, *Appl. Phys. Lett.* **80**, 1909 (2002).
- <sup>13</sup>L. Bergman, X. B. Chen, J. Huso, J. L. Morrison, and H. Hoock, *J. Appl. Phys.* **98**, 093507 (2005).
- <sup>14</sup>X. T. Zhang, Y. C. Liu, Z. Z. Zhi, J. Y. Zhang, Y. M. Lu, D. Z. Shen, W. Xu, G. Z. Zhong, X. W. Fan, and X. G. Kong, *J. Phys. D* **34**, 3430 (2001).
- <sup>15</sup>V. V. Ursaki, I. M. Tiginyanu, V. V. Zalamai, E. V. Rusu, G. A. Emelchenko, V. M. Masalov, and E. N. Samarov, *Phys. Rev. B* **70**, 155204 (2004).
- <sup>16</sup>V. V. Zalamai, V. V. Ursaki, E. V. Rusu, P. Arabadji, I. M. Tiginyanu, and L. Sirbu, *Appl. Phys. Lett.* **84**, 5168 (2004).
- <sup>17</sup>T. Makino, Y. Segawa, and M. Kawasaki, *J. Appl. Phys.* **97**, 106111 (2005).
- <sup>18</sup>Z. B. Gu, C. S. Yuan, M. H. Lu, J. Wang, D. Wu, S. T. Zhang, S. N. Zhu, Y. Y. Zhu, and Y. F. Chen, *J. Appl. Phys.* **98**, 053908 (2005).
- <sup>19</sup>C. L. Du, Z. B. Gu, M. H. Lu, J. Wang, S. T. Zhang, J. Zhao, G. X. Cheng, H. Heng, and Y. F. Chen, *J. Appl. Phys.* **99**, 123515 (2006).
- <sup>20</sup>R. Cebulla, R. Wendt, and K. Ellmer, *J. Appl. Phys.* **83**, 1087 (1998).
- <sup>21</sup>M. C. Klein, F. Hache, D. Richard, and C. Flyzanis, *Phys. Rev. B* **42**, 11123 (1990).
- <sup>22</sup>R. Loudon, *Adv. Phys.* **13**, 423 (1964).
- <sup>23</sup>J. F. Scott, T. C. Damem, W. T. Silfvast, R. C. C. Leite, and L. E. Cheesman, *Opt. Commun.* **1**, 397 (1970).
- <sup>24</sup>A. Ingale, M. L. Bansal, and A. P. Roy, *Phys. Rev. B* **40**, 12353 (1989).